LM-04K150
December 13, 2004

Probing the Elastic-Plastic, Time-Dependant Response of Test Fasteners using Finite Element Analysis (FEA)

ML Renauld and H Lien

Mark L. Renauld and Hue Lien[1]

Probing the Elastic-Plastic, Time-Dependent Response of Test Fasteners using Finite Element Analysis (FEA)

Reference: Renauld, M.L. and Lien, H., **"Probing the Elastic-Plastic, Time-Dependent Response of Test Fasteners using Finite Element Analysis (FEA),"** Third Symposium on Structural Integrity of Fasteners Including the Effects of Environment and Stress Corrosion Cracking (SCC), Toor, PM and Barron, BJ, Eds., American Society for Testing and Materials, West Conshohocken, PA, 2004.

Abstract: The evolution of global and local stress/strain conditions in test fasteners under test conditions is investigated using elastic-plastic, time-dependent finite element analyses (FEA). For elastic-plastic response, tensile data from multiple specimens, material heats and test temperatures are integrated into a single, normalized flow curve from which temperature dependency is extracted. A primary creep model is calibrated with specimen- and fastener-based thermal relaxation data generated under a range of times, temperatures, stress levels and environments. These material inputs are used in analytical simulations of experimental test conditions for several types of fasteners. These fastener models are constructed with automated routines and contact conditions prescribed at all potentially mating surfaces. Thermal or mechanical room temperature pre-loading, as appropriate for a given fastener, is followed by a temperature ramp and a dwell time at constant temperature. While the amount of thermal stress relaxation is limited for the conditions modeled, local stress states are highly dependent upon geometry (thread root radius, for example), pre-loading history and thermal expansion differences between the test fastener and test fixture. Benefits of this FE approach over an elastic methodology for stress calculation will be illustrated with correlations of Stress Corrosion Cracking (SCC) initiation time and crack orientations in stress concentrations.

Keywords: Finite Element Analysis, FEA, fastener, SCC, elastic-plastic

Engineer and Engineer, Lockheed-Martin Corporation, Box 1072, Schenectady, NY 12301-1072

1.0 Introduction

The performance of bolted closures is often reliant upon fasteners to maintain joint integrity throughout the range of a typical and off-nominal service conditions. This may entail adequate pre-load to prevent joint separation during shock/seismic events, ability to withstand cyclic loads and/or adequate resistance to environmental degradation. Demonstration of structural adequacy may be achieved using simple elastic stress calculation methods, such as Reference [1], for test specimens and service hardware. However as economic and performance metrics continue to push mechanical designs, more in-depth analytical assessments are often required to ensure structural adequacy. Redundancy and safety margin are particularly important where consequences of mechanical failure are substantial [2]. As analytical requirements have grown, computational capability and software developments have evolved such that the ability to more fully simulate structural response and material deformation has been enabled. For example, finite element models can now be readily constructed for stress concentration comparisons with handbook elastic stress calculations [3, 4]. These computational advances have provided deeper insight into mechanisms and behaviors, thereby providing confidence in extended service lives and reduced cost designs.

Stress concentration locations in fasteners continue to receive significant attention since the amplification of nominal shank stresses often make thread roots and head fillets limiting design locations. Two-dimensional and three-dimensional FEA has shed additional light on the local stress states developed under elastic [3, 4] and elastic-plastic assumptions [5]. Additionally, the influences of friction [5] and of thermal vs mechanical bolt pre-loading conditions [6, 7] have been studied. As more in-depth investigations are pursued the effort required for geometric representation and finite element discretization correspondingly increase. This time investment has been addressed using submodeling and automated meshing techniques [8, 9], thereby controlling the time costs associated with the advanced analyses.

In this paper, two-dimensional, elastic-plastic finite element modeling is used to explain observed SCC initiation behavior of test fasteners in pressurized water. For this set of fasteners, conventional handbook elastic stress calculations do not explain the initiations times measured at different locations in the same fastener nor could the orientation of the observed cracks be explained. Simplifying geometric assumptions were used to enable two-dimensional, axisymmetric modeling techniques and automated scripts were developed for finite element mesh generation to ensure consistency among models and expedite model creation. Material deformation was modeled as elastic-plastic to more accurately represent stress concentrations which do not remain elastic, thereby also capturing any path dependency effects during fastener pre-loading. Model solution included stress relaxation during the elevated temperature exposure using a primary creep model to elucidate potential effects of relaxation on observed behaviors. The ABAQUS/CAE pre-processor in conjunction with the ABAQUS finite element solver and ABAQUS/VIEWER post-processor were used throughout the study.

2.0 Material Properties

2.1 Tensile Properties

The properties for traditional elastic FEA (elastic modulus, mean coefficient of thermal expansion and Poisson's ratio) were extracted from data fits with second order polynomials as a function of temperature; the exception being Poisson's ratio which was maintained at 0.3. The elastic-plastic properties were established from tensile tests covering multiple material heats, strain rates and temperatures. The yield strength dependency with temperature was adequately modeled by a second order polynomial and the entire tensile curves were normalized by the heat- and temperature-dependent yield stress and yield strain. These data reduction techniques collapsed all tensile curves into a "universal" curve to which a 4^{th} order polynomial was fit, as illustrated in Figure 1. Heat- and temperature-dependent tensile curves were then "backed out" from this "universal" curve and true stress-true plastic strain pairs were calculated for the ABAQUS input decks.

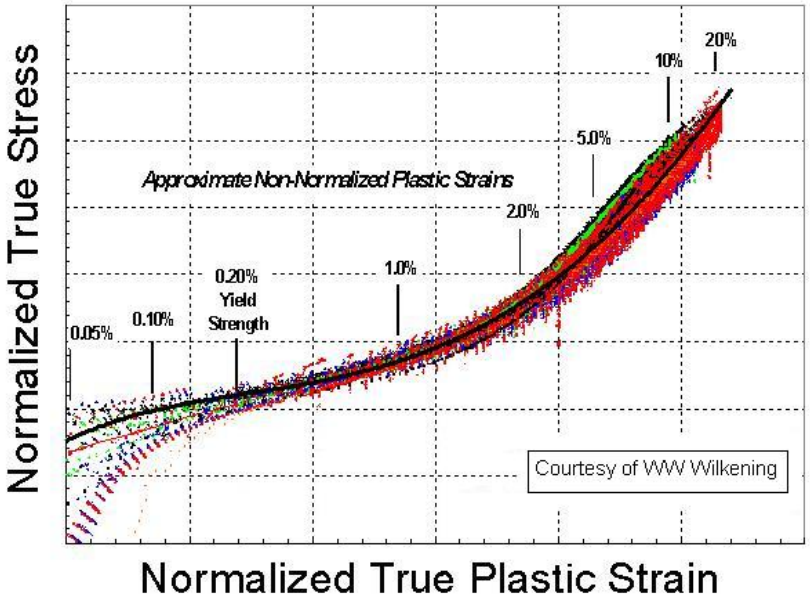

Figure 1. Tensile response determined from multiple specimens, material heats and temperatures are collapsed into a "universal" curve to ensure smooth elastic-plastic response and temperature transitions in the finite element simulations.

2.2 Stress Relaxation Properties

Time-dependent deformation was included in the finite element analyses to evaluate any changes in the magnitude or location of the stresses produced during preloading and heating to elevated temperatures. A relaxation model, based on a conventional primary creep formulation, was developed for the fasteners but not the fixtures since the larger cross-sectional area of the fixtures results in a much lower nominal and concentrated stress. The lower stresses, in turn, produce much less relaxation. A comprehensive set of fastener- and specimen-based relaxation data were included such that experimental information over a range of conditions were considered: temperatures, environments, stress levels and initial strain levels for elastic as well as elastic-plastic preloading. The database was used to regress coefficients n, m, Q and $\dot{\varepsilon}$ for the primary creep relationship expressed in Eq (1):

$$\dot{\varepsilon} = \dot{\varepsilon}_o \sigma^n t^m e^{\frac{-Q}{RT}} \tag{1}$$

The experimental stress relaxation data was converted to strain rates by calculating stress reductions over a given time interval, $d\sigma/dt$, and dividing by the temperature-adjusted elastic modulus to provide strain rates, $\dot{\varepsilon}$. The ability of this model form to fit the experimental data is illustrated in Figure 2. Eq. (1) was then modified to match the Power-law model creep model embedded in ABAQUS [11] written as:

$$\dot{\varepsilon} = A\sigma^n t^m \tag{2}$$

where n and m have the same values as in Eq. (1) but A has the temperature dependency shown in Eq. (3):

$$A = \dot{\varepsilon}_o e^{\frac{-Q}{RT}} \tag{3}$$

The FE input decks contained temperature independent values of n and m with temperature dependent values of A given by Eq. (3).

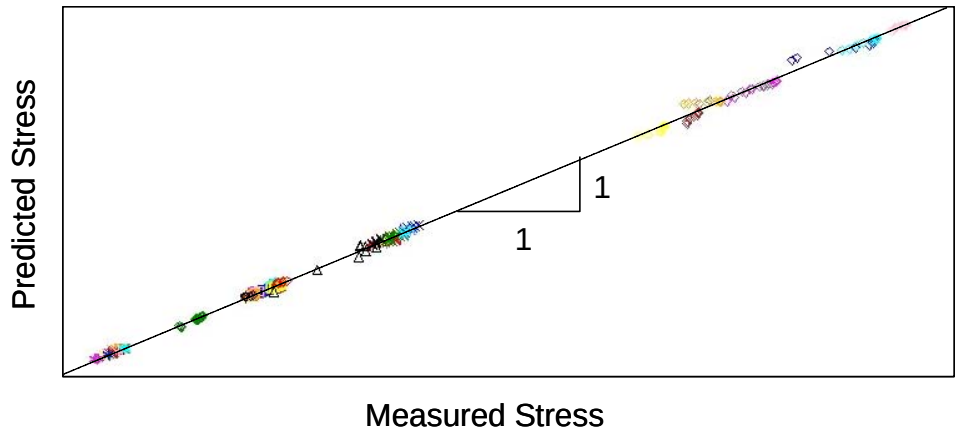

Figure 2. The primary creep equation shown in Eq (1) provides a reasonable correlation of measured stress relaxation data generated at multiple temperatures, in various environments and with a range of initial stress levels.

3.0 FEM Development

3.1 General Modeling Assumptions

A series of finite element models using the finite element code ABAQUS were developed to perform a controlled study to evaluate behavior of two fastener types, a bolt and a stud. All the FEM models developed consist of similar components: a threaded fastener (stud or bolt), nut(s), and spacer. 2D axisymmetric finite element models were generated using quadratic hybrid continuum elements for both fasteners and associated fixtures.

The models were generated using an automated subroutine to replicate the same controlled mesh near the root of the thread for various models used. Figure 3 illustrates this process in which the geometry, FE mesh, and contact definition were consecutively created. The geometry was created based on parameterized dimensions for ease of performing geometric studies. These parameterized dimensions include standard thread dimensions obtained from Reference [11]. The geometry was also automatically partitioned in CAE to aid in creating a replicable mesh in which small elements are positioned at the thread root. The subroutine also defines the contact surfaces of each individual thread to create contact interaction to eliminate errors from occurring while defining the contact pairs.

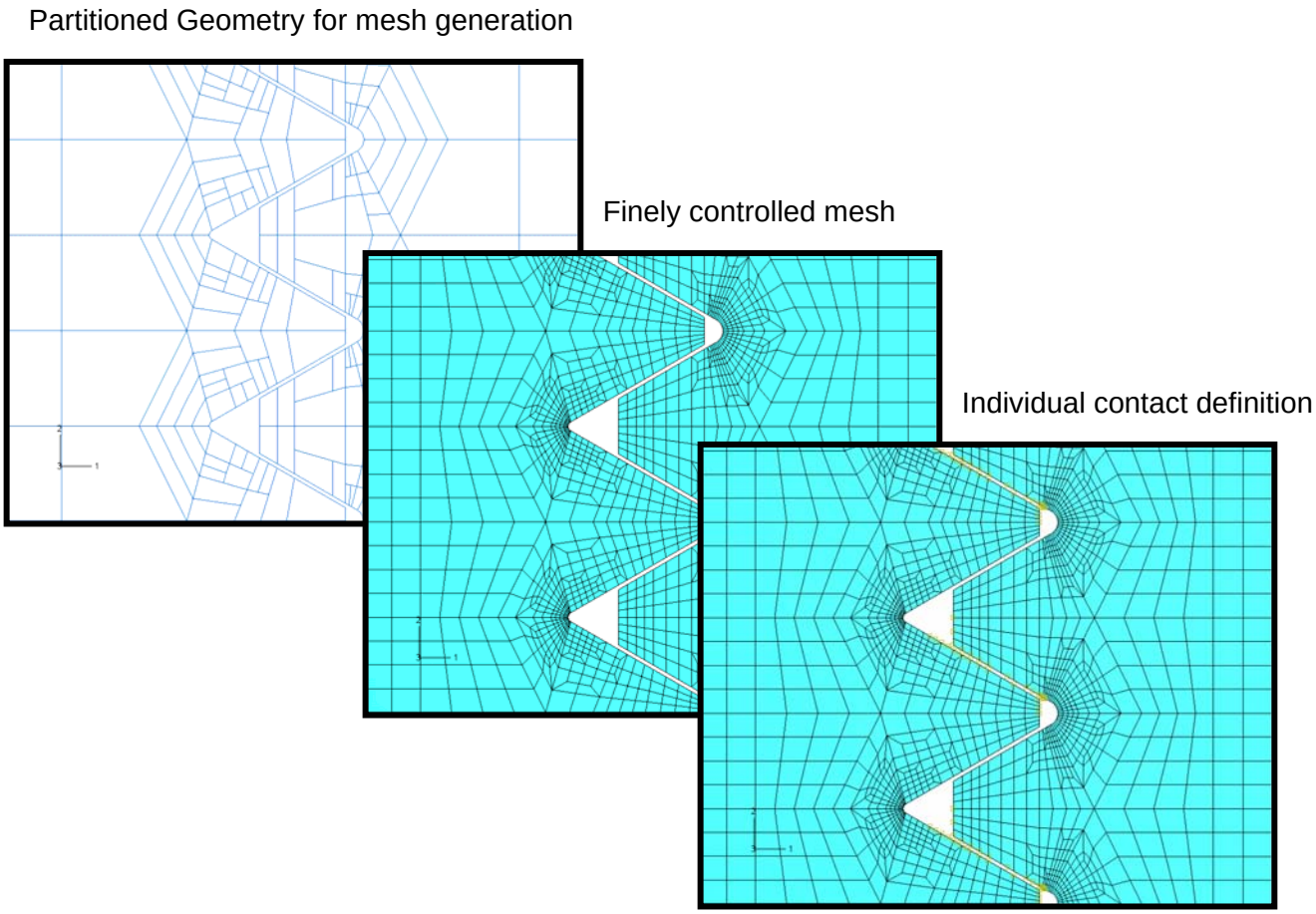

Figure 3. Automated model generation process.

Since the models developed were axisymmetric, the threads were modeled as annular rings in lieu of the actual helical configuration in threads. This limited the ability to make minor changes in the position the nut relative to the fastener threads for preloading the model. The nut could not be rotated and only thread pitch increments could be used which are too coarse to meet desired preload levels. Therefore, slight adjustments were made to the height of spacer to account for this effect and control the amount of preload. The model parts were assembled with a series of contact surfaces to provide a compression/tension path across the mating surfaces of the threads in the nut and fastener, nut and spacer, and the upper nut / bolt head and spacer.

3.2 Experimental and Analytical Fastener Preloading

Experimentally, the test bolts are thermally loaded by a heater inserted into a center heater hole, as illustrated in Figure 4, to heat and expand the bolt. When elongated, the bolt is threaded further into the nut eliminating clearance between the bottom of the bolt head and the top of the spacer. Upon cooling to RT, a tensile bolt preload and compressive fixture preload are achieved via an elongation of the bolt. Analytically, a similar procedure is followed beginning with raising the bolt temperature, activating the contact surface between the bolt head and spacer and cooling the bolt to room temperature. The amount of final bolt elongation is controlled by the amount of initial interference between the bolt head and spacer. This initial interference is increased or decreased by adjusting the spacer height such that the analytically preloaded bolt elongation matches the experimental elongations. Sensitivity studies indicated a small change (<2%) in head fillet and thread root stresses for the range of measured elongations (~10% variation) in “duplicate” bolts, therefore an average elongation was used for the bolts. Once pre-loaded, the temporary springs are deleted, the entire assembly is raised to test temperature and held, at temperature, for the length of time the experimental fasteners were exposed.

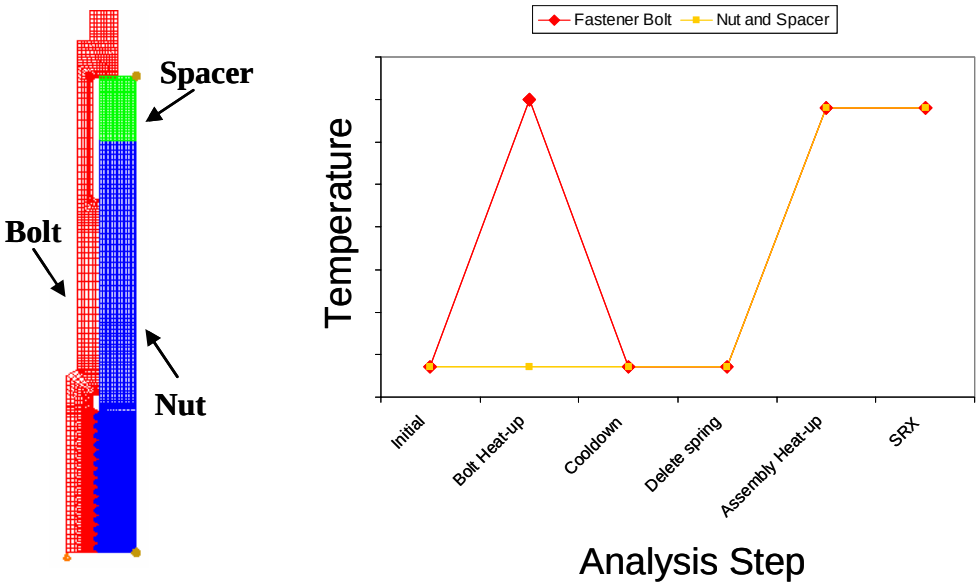

Figure 4. **Thermal preloading of a test bolt whereby the bolt is elongated, the bolt head/spacer contact pair is activated and the bolt is cooled.**

The studs were experimentally preloaded at RT by applying an external load to threads protruding above the top nut and by resisting this load on top of the compression sleeve, as illustrated in Figure 5. With this tensile load, a minor torque is applied to the top nut after which the external load is removed. The finite element procedure mimics the experimental process except the nut torque is replaced by contact surface activation and resolution of the top nut / sleeve interference. Strain gages were mounted at 90° circumferential positions along shank portions of four studs to monitor strain during these preloading steps. Figure 6 shows the average of the four strain gages on the individual studs along with finite element calculations. Note that Figure 6 shows two analytical paths resulting from using friction coefficients of 0.1 and 0.3. Although a coefficient of 0.1 appears to show improved correlation with strain gage measurements, the coefficient was set at 0.3 for consistency with the stud analyses. The difference in thread root stresses was a couple percent for the two different friction coefficients.

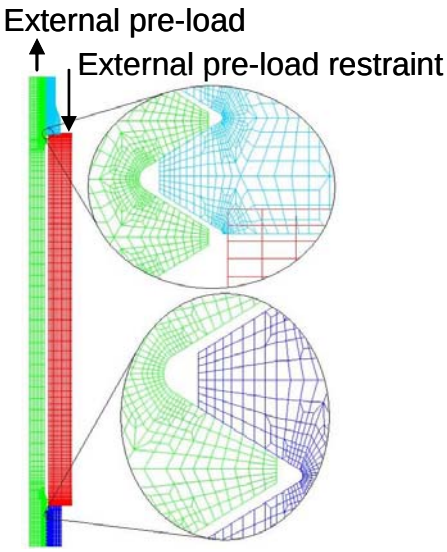

Figure 5. **The stud is preloaded by an external mechanical load, nut torque and external force removal.**

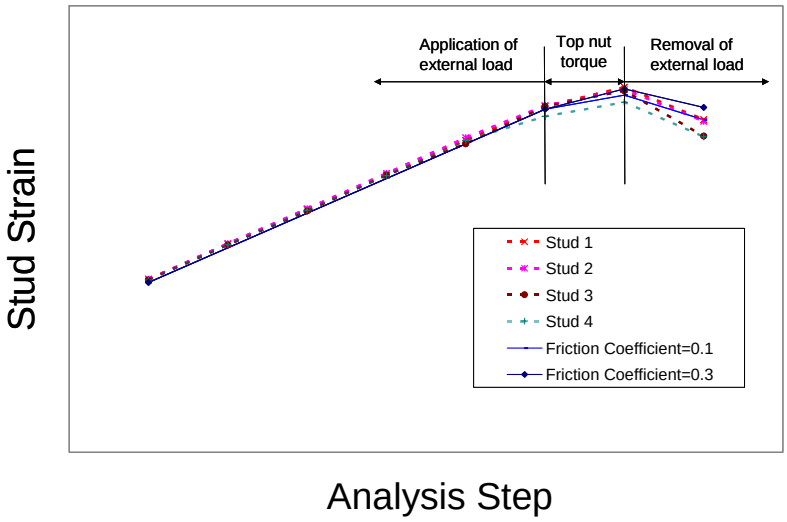

Figure 6. Average stud strains recorded during preloading compare well to finite element predictions.

4.0 FEM Results

With the proper loading sequence established, finite element model solution were performed to investigate the stress developed in a fastener component over a cycle of use, i.e., from initial preloading through an entire exposure at test temperature. Figure 7 illustrates the stress evolution at the thread root and fillet at the bolt head. Figure 7(a) illustrates the fastener model at the start on the analysis. An initial interference fit was modeled to allow for adjustment to the preload. Figure 7(b) shows the interference between the head and spacer is cleared during the thermal loading process. The contacting surface is activated after the interference is resolved to provide the tension/compression path in the point. Figure 7(c) and (d) illustrate the stress predictions at the head fillet and thread root at the end of pre-load and high temperature exposure, respectively. No stress was developed during the initial thermal loading cycle until the simulation step of fastening the nut was performed, replicated by activating the contact surface between the head fillet and the spacer to establish a compression path. The maximum stresses are achieved at room temperature after preloading. On raising the assembly to test temperature, the bolt preload is reduced by approximately 20%. During the elevated temperature exposure wherein the relaxation model is activated, very small changes occur in the magnitude of the bolt load as well as thread root and head fillet stresses. Stress relaxation does not affect the orientation of maximum stress in the features, nor does it change the prediction of higher stress magnitudes in the head fillet than in the thread root.

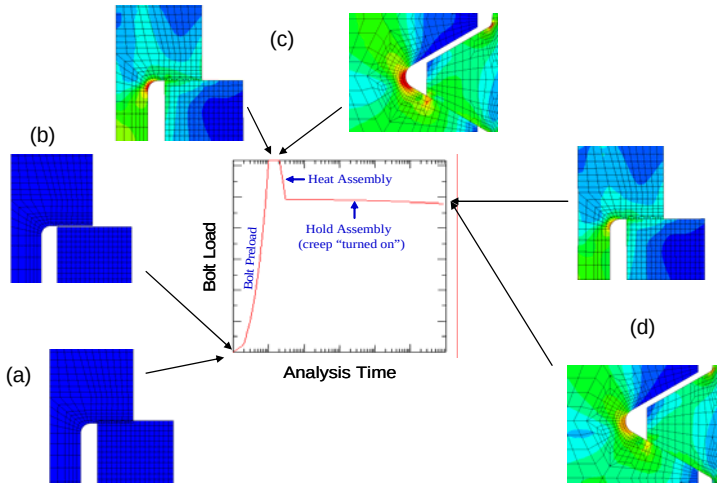

Figure 7. Stress evolution in the head fillet and first engaged thread for the bolt. (a) shows the model with the initial interference fit, while (b) illustrates the analytical event of during the thermal preloading cycle. (c) and (d) provides stress prediction at two different stages in the analysis.

For the mechanically preloaded stud, the loading response is much more complex due to the external force and nut torquing. Figure 7 indicates that stress is developed in both the lower and upper thread root of the stud during mechanically tensioning the stud, with the lower thread stress increasing more rapidly primarily due to its higher elastic stress concentration factor. Nut torquing (contact surface resolution) induces limited amounts of additional stress since this procedure is primarily intended to maintain, not significantly increase the stud load, therefore the torque applied to the nut is quite small. As the external load is removed, the load distribution in the tension/compression path is redistributed, such that the maximum local thread stress location changes from the bottom to the top first engaged thread. Simple elastic calculations using stress concentration factors do not include this history dependency and suggest the lower thread stress is higher after preloading.

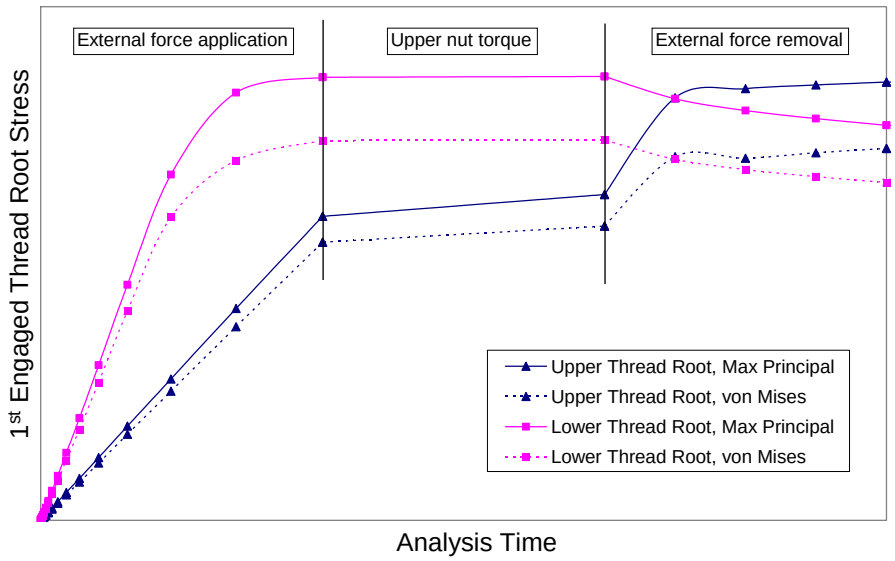

Figure 8. Stress evolution in the upper and lower 1st engaged stud threads during room temperature preloading.

Similar to the pre-processing phase of the analysis, an automated script was used to post-process the finite element results since large quantities of data are produced for even a single analysis. The automated script was used to extract specific outputs of interests from the different finite element results. Figure 9 illustrates an example of the data collected during this automation process, where a variety of stress and strain quantities during different stages of the analysis were obtained. Similar

results output were gathered from multiple analyses and at different locations. The computer program, written in Python to be used in conjunction with ABAQUS CAE, provided a tool to quickly compile similar results from the different models, while minimizing human error, for use in comparative studies between multiple locations in a single fastener and between the stud and bolt. The locations and orientations of the extracted maximum principal stress values were used to explain experimental findings.

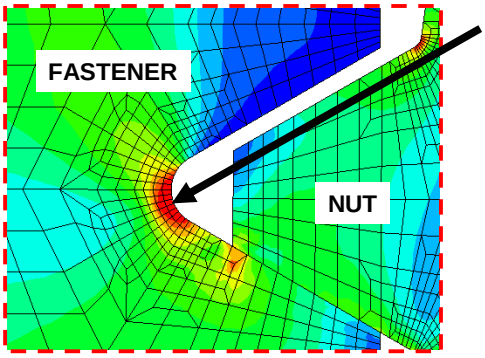

	Timestep1		Timestep2		Timestep3	
	Node	value	Node	value	Node	value
Von Mises	547	VM1	546	VM2	545	VM3
Max Principal	553	MP1	553	MP2	264	MP3
Pressure	553	P1	262	P2	262	P3
Strain Energy Density	551	SED1	551	SED2	264	SED3
Plastic Dissipation Energy Density	547	PDED1	547	PDED2	547	PDED3
Total Equivalent Strain	551	TES1	551	TES2	551	TES3
Equivalent Plastic Strain	547	EPS1	547	EPS2	547	EPS3
Max Principal Total Strain	547	MPTS1	547	MPTS2	547	MPTS3
Max Principal Plastic Strain	547	MPPS1	547	MPPS2	547	MPPS3

Figure 9. Automated scripts were developed to extract maximum stress & strain quantities in the thread roots and head fillets.

5.0 Application of FEA Results

The elastic-plastic finite element results were compared with experimental observations which could not be explained from simple handbook elastic calculations, for this set of fastener data. Figure 10 illustrates the crack orientations observed in the thread roots and a corresponding FE fringe plot of maximum principal stress. The macroscopic angle of crack initiation and growth rotates from nearly perpendicular to the free surface of the fastener for the first unengaged thread to around 30° along the pressure flanks for the second and third engaged thread. The maximum principal stress predicted by the elastic-plastic finite element model rotates in a similar fashion. An elastic K_t-based calculation using Reference [1], for instance, would suggest highest stresses (and cracking) at the root of the thread for all threads. Note that in Figure 10, the FEM does not represent the specific test fastener and fixture but the trend of observed crack orientation changes and predicted stress rotation is generally observed experimentally and analytically.

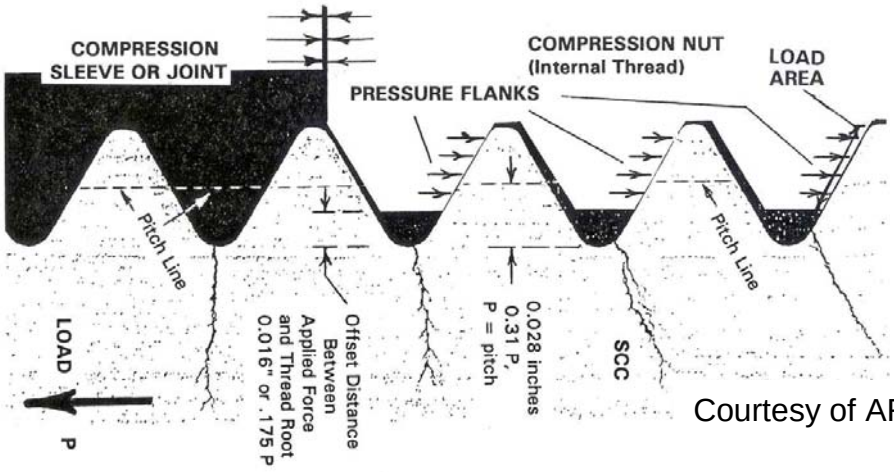

Courtesy of AR Kephart

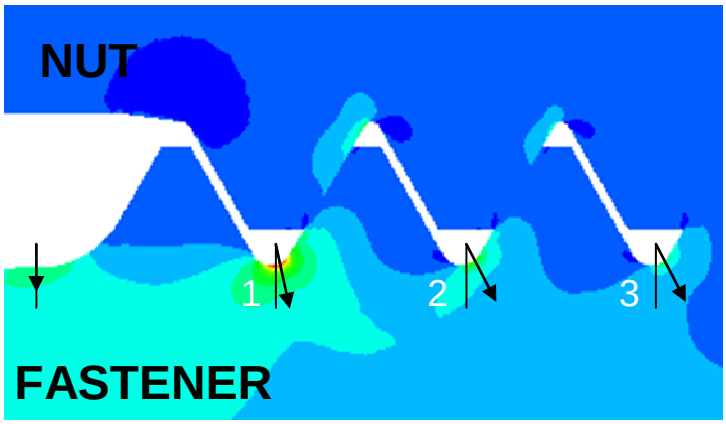

Figure 10. The elastic-plastic FEA results accurately predict the orientation of stress corrosion cracks for un-engaged and engaged threads.

Figure 11 plots the measured SCC initiation time as a function of elastically calculated stresses and the maximum principal stresses extracted from the elastic-plastic FEA using the automated script. For these bolts and studs, elastic stresses do not appropriately predict the relationship between local stress and measured SCC initiation time. Locations with higher elastic stresses within the same fastener demonstrate longer initiation times. Conversely, the elastic-plastic FE calculated stress correctly orders the observed initiation times. The maximum principal stress does not collapse all life data to a single curve because all fasteners were not tested under identical conditions (temperature, environment) and there is inherent data scatter in the initiation times even under identical test conditions.

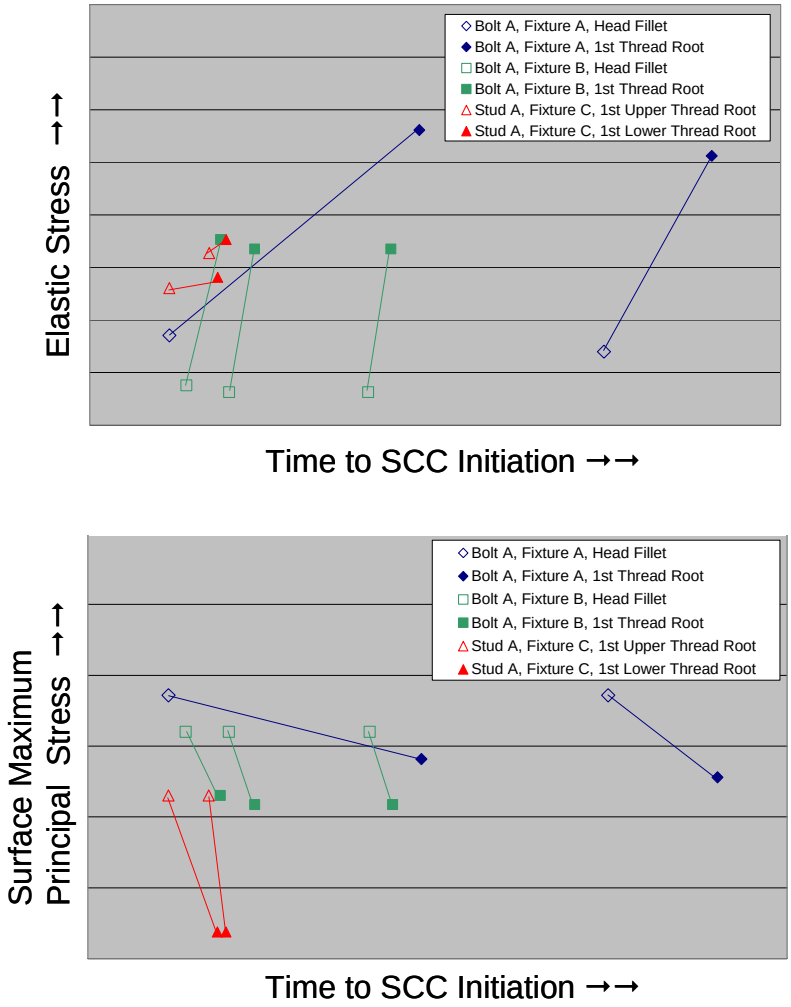

Figure 11. **For this set of test fasteners, elastically-calculated local stresses do not accurately predict life trends, i.e., locations of higher stresses demonstrate longer lives for the same test fastener. The elastic-plastic FEA results correctly order the SCC initiation times.**

6.0 Summary

Elastic-plastic finite element analysis has been used to replicate the loading procedure and elevated temperature exposure (with stress relaxation) of test fasteners under test conditions. Automated scripts were developed to expedite finite element meshing and post-processing of FEA results. By tracking the history-dependent evolution of local stress states at thread roots and bolt head fillets, observed SCC characteristics can be explained. In particular, the measured time to SCC initiation can be ranked by elastic-plastically calculated stresses. Also, the orientations of stress corrosion cracks within thread roots can be correlated with the locations of maximum stress.

Acknowledgements
The authors appreciate assistance provided by Dr. Weldon Wilkening for the elastic-plastic curve data reduction process and by Mr. Alan Kephart for his experimental test results and insight.

7.0 References

[1] Peterson, R.E., Stress Concentration Factors, John Wiley & Sons, Inc, New York, 1974.

[2] McVicker, J.P., Conner, J.T., Hasrouni, P.N. and Reizman, A., “Simplified Failure Sequence Evaluation of Reactor Pressure Vessel Head Corroding in-Core Instrumentation Assembly,” PVP-Vol. 318, Structural Integrity of Pressure Vessels, Piping, and Components, 1995, p. 25-31.

[3] Srinivasan, G. and Lehnhoff, T.F., “Bolt Head Fillet Stress Concentration Factors in Cylindrical Pressure Vessels,” PVP-Vol. 415, Recent Advances in Solids and Structures, 1999, p. 171-178.

[4] Lehnhoff, T.F. and Bunyard, B.A., “Bolt Thread and Head Fillet Stress Concentration Factors,” Journal of Pressure Vessel Technology, Vol. 122, 2000, p. 180-185.

[5] Fukuoka, T. and Takaki, T., “Elasto-Plastic Anlysis of Bolted Joint during Tightening Process,” DE-Bol. 105, Reliability, Stress Analysis, and Failure Prevention Issues in Adhesive and Bolted Connections, 1999, p. 151-156.

[6] Fukuoka, T. and Xu, Q., “Analysis of the Tightening Process of Bolted Joint with a Bolt Heater,” PVP-Vol. 367, Analysis of Bolted Joints, 1998, p. 53-59.

[7] Xu, Q. and Fukuoka, T., “Finite Element Simulation of the Tightening Process of Bolted Joint with a Bolt Heater,” PVP-Vol. 405, Analysis of Bolted Joints, 2000, p. 71-78.

[8] Kim, T.-W., Kim, Y.-D. and Lee, B.-Y., “Finite Element Analysis of Bolted Joint Assembly of Nuclear Power Plants, PVP-Vol. 368, Analysis and Design of Composite, Process, and Power Piping and Vessels, 1998. p. 185-189.

[9] Kinney, P. and Strenski, D., “Three Dimensional Threaded Fastener Meshing Algorithm,” Proceedings of the Sumposium on Solid Modeling and Applications, 2001, p. 71-77.

[10] ABAQUS/Standard User’s Manual, Volume II, Version 6.3, Hibbitt, Karlsson and Sorensen, Inc., 2002.

[11] Machinery’s Handbook, 25th ed., Industrial Press, New York, 1996.